Journal of the Meteorological Society of Japan, Vol. 73, No. 2B, pp. 427–442, 1995

Doppler Radar Observation of the Structure and Characteristics of Tropical Clouds during the TOGA-COARE IOP in Manus, Papua New Guinea — Three Case Studies on November 23 and December 16, 1992 —

By Nobuhiro Takahashi[1] and Hiroshi Uyeda

Department of Geophysics, Faculty of Science, Hokkaido University, Sapporo 060, Japan

(Manuscript received 1 August 1994, in revised form 27 February 1995)

Abstract

During the TOGA-COARE intensive observation period (IOP), many types of clouds were observed around Manus Island, Papua New Guinea, by X-band Doppler radars. This paper analyzes several characteristics of three types of tropical convective clouds, an isolated echo cell and two types of rainbands. The common characteristics, from the viewpoint of echo area, echo-top height and maximum reflectivity, in association with the development process are that 1) the peak of maximum reflectivity appeared in the early stage in the lower-level circulation, 2) the peak of the maximum echo top height appeared shortly after the maximum reflectivity caused by a development of upper-level circulation, and 3) the maximum echo area appeared at a later stage because of the appearance of anvil clouds.

In the case of the isolated echo, the above-mentioned characteristics were examined with kinematics in detail. The development of low-level circulation into upper-level circulation appeared successively and coexisted in the case of an isolated echo. In all cases, a strong reflectivity core appeared at the lower altitude, indicating the effectiveness of the warm-rain process. The echo-top height did not increase continuously to the maximum height; stable echo-top heights appeared during the echo development. This tendency was common to all cases of rainband. Anvil clouds contributed to the extension of the upper tropospheric cloud area in the later stage of its life cycle and formed a stratiform echo.

Rainbands are categorized as non-squall type from the GATE criteria (Barnes and Sieckman, 1984; Houze, 1977). Both rainbands developed parallel to the low-level shear vector. The first case was slow-moving: the rainband had a clear leading edge and continuous rear-to-front flow to maintain the circulation during the mature stage. The second case was relatively fast-moving: it had intermittent rear-to-front flow. These are somewhat different characteristics from rainbands during GATE. Convective outflows were also observed in all cases. In particular, gust fronts were observed in the rainband cases. The gust front in the second rainband had a thickness of 0.5 to 1.0 km, and a propagation speed of 8 to 10 m/s, which was slightly faster than the rainband's propagation speed.

1. Introduction

Organized convective systems occur over the tropical oceans in cloud clusters which consist of several cumulonimbi and stratiform clouds with horizontal dimension of 200–1000 km. One of the most comprehensive observations of the structure of tropical clusters and mesoscale features was performed during GATE (Global Atmospheric Research Program's Atlantic Tropical Experiment) in 1974 over the tropical Atlantic Ocean.

In the GATE experiment, cloud clusters were categorized into two types: 'squall' and 'non-squall': a squall line has a rapid propagation speed and an arc-shaped leading edge (Houze, 1977; Leary and Houze, 1979b). Houze and Rappaport (1984), on the other hand, pointed out a slow-moving oceanic squall line. The non-squall convective clouds have a slow propagation speed and an ambiguous leading edge (Zipser *et al.*, 1981; Leary and Houze, 1979a). Also, the differences between squall lines and non-squall clouds are that the convective lines (leading edges) of squall lines are perpendicular to the low-level vertical wind shear (*e.g.*, surface to 600 hPa), while the convective lines are parallel to the low-level vertical wind shear in the non-squall clouds.

Most of the GATE squall lines were generated over the African continent where a relatively dry

1 Present affiliation: Communications Research Laboratory.

layer exists in the middle level (below 700 hPa). Barnes and Siekmen (1984) pointed out that the middle-level dry layer characterized the squall lines; it contributes to the development of a cold pool at the leading edge and intensify gust fronts ahead of squall lines. A numerical investigation by Tao and Simpson (1989) emphasized the importance of the cold pool and convective outflow to maintain squall lines. The results of the GATE experiment were summarized by Houze and Betts (1981). The characteristics of African squall lines were confirmed by a three-dimensional kinematic analysis of dual Doppler radar observations of topical squall lines over the African continent during COPT 81 (Chong *et al.*, 1987).

Besides the experiments over the Atlantic Ocean, several experiments investigated tropical convective systems, especially over the western Pacific Ocean where the sea surface temperature is the highest in the world (the so called "warm-water pool"). In the winter of 1978/79, WMONEX (Winter Monsoon Experiment) was performed over the sea to the north of Borneo Island. Houze *et al.* (1981) analyzed mesoscale convective systems which had a regular diurnal cycle. In their study, the diurnal cycle was caused by interaction between sea/land breezes and monsoonal winds, but convective systems also contributed to the intensification of the sea/land breezes.

Along the northern coast of the Australian continent, several experiments were performed using dual Doppler radars. Keenan and Rutledge (1993) observed a short-lived squall line that was generated under an environmental condition of low-CAPE (Convective Available Potential Energy) ($\sim$360 J/kg) and low vertical wind shear ($\sim$12 m/s (4000 m)$^{-1}$).

These studies over and around the Pacific Ocean showed different types of tropical mesoscale convective systems from those which were observed in GATE, but convective systems were generated very close to the Australian continent or the maritime continent. It is necessary to observe a region far away from continents in order to understand the cloud clusters generated over the warm-water pool where the atmospheric structure is thought to be more moist at lower levels than in other regions.

Mori (1992) described subsystems of a cloud cluster using a conventional radar mounted on a research vessel at the ITCZ of the western Pacific Ocean. His study suggested that detailed investigation of cloud cluster subsystems is important to clarify the organization mechanism of cloud clusters.

During the ten-week period beginning November 12, 1992, the Intensive Observation Period (IOP) of the TOGA-COARE (the Tropical Ocean-Global Atmosphere program, a Coupled Ocean-Atmosphere Response Experiment) made a comprehensive observation of convective systems and air-sea interaction around the western Pacific Ocean warm-water pool. In these observations, two X-band Doppler radars were used on a small isolated tropical island, Manus Island (2°S, 147°E), Papua New Guinea. The major purposes of the Doppler radar observation were to clarify the kinematic structure of tropical convective clouds which consist of cloud clusters and to determine the three-dimensional distribution of precipitation. An overview of the dual Doppler radar observation on Manus Island is shown by Uyeda *et al.* (1995).

There have been few observations performed using Doppler radars in this area. During the TOGA-COARE observations, many kinds of clouds were observed by Doppler radars, such as squall lines, convective clouds and stratiform clouds associated with cloud clusters, isolated convective clouds over the island in the daytime, and so on.

In this study, three case studies of tropical clouds with different horizontal scale are analyzed using Doppler radar data obtained during TOGA-COARE IOP in order to accumulate the basic characteristics and kinematics of tropical convective clouds, such as 1) the time and geometrical scale of several types of clouds, 2) the cloud physical and kinematic processes of tropical cloud development, and 3) the organization processes of tropical clouds. The first case is an isolated convective echo, and the second and third cases are rainbands with lengths of $\approx$ 50 km and $\approx$ 100 km. There are few studies on the life cycle and kinematic structure of tropical isolated echoes compared with mesoscale rainbands such as squall lines and non-squall rainbands. This may be because isolated echoes are less important than organized convective systems and they are thought to have relatively simple structures. However, we think it is very important to understand the behavior of isolated clouds without organization, because isolated echoes simply reflect the environmental atmospheric conditions such as atmospheric stability.

Hence, in this paper we first analyze an isolated convective cloud observed on November 23, 1992, because it did not interact with clouds that were located far from it, and it is considered to have a relatively simple structure. The isolated echo was generated on the island and was not related to cloud clusters. This analysis revealed the basic characteristics of tropical convective clouds, for example, the horizontal and vertical dimensions of each cloud, the duration of the cloud's life, and the transition of the vertical circulation inside the cloud during its life cycle. After that, we analyze the mesoscale rainbands that were observed on December 16. One initiated at the western edge of a mesoscale cloud cluster during the day time, and after that another rainband developed.

In the second and third cases, convective outflows

(gust fronts) were clearly observed by Doppler radar. It is well known that low-level convergence is one of the major forces that generates new clouds and maintains their development. In mid-latitudes, the low-level convergence of synoptic frontal systems associated with extratropical cyclones forces the formation of wide and narrow rainbands (*e.g.*, Hobbs and Persson, 1982). Convective outflows are also major forces behind mesoscale and/or cloud scale convergence for mid-latitudinal mesoscale convective systems. In the tropical region, as mentioned above (Tao and Simpson, 1989), convective outflows (gust fronts) help maintain the tropical mesoscale convective systems such as squall lines and non-squall rainbands. In this paper, we describe the magnitude and thickness of a gust of a tropical convective rainband, and we examine the possible formation mechanisms of convective outflow in tropical clouds.

In order to clarify the common characteristics of the three different scale echoes, we compare them in terms of the life cycles: transitions of vertical and horizontal development, using the results of single Doppler radar data analysis.

2. Data sources and analysis method

The main source of data used in this study was derived from Doppler radar (Hokkaido University X-band Doppler radar) observations. Doppler radars provide data on reflectivity, Doppler velocity, and the spectral width of Doppler velocity. The observation range is 60 km with a resolution of 250 m in range and 1.5° in azimuth. The operation modes were basically selected at 15-minute intervals of volume scan (with PPI scans at 14–16 elevation angles) in order to survey three-dimensional structures, and for dual Doppler analysis. Several RHI scans were obtained intermittently, and, to examine short-term cloud variations, data were collected at 5-minute intervals with a few PPI and RHI scans whenever necessary.

In the analysis of isolated convective clouds, short-interval data were utilized in order to examine the detailed development of the echo. In this case, the antenna was scanned at 5-minute intervals in the PPI mode (elevation angle = 3°) and also made one or two RHI scans pointing in the direction of the target cloud. On the other hand, for the analysis of rainbands, the normal mode (15-minute intervals) observation data were used.

In the case of the isolated echo, the temporal variation of echo area (> 19 dBZ) of 3° elevation data and the 19 dBZ echo height were analyzed and the radial divergence field was also calculated from the Doppler velocity data. In this case, radial divergence means the radial gradient of the Doppler velocity, not the actual horizontal divergence. If the kinematic structure of an isolated echo was axisymmetric or two-dimensional, the radial divergence value could be useful to deduce the actual divergence. Rotunno *et al.* (1988) reviewed that short-lived thunderstorms have relatively simple life cycles with simple circulation structures. Tabata *et al.* (1989) analyzed the wind field of a mid-latitude single-cell cloud using dual Doppler radars. In their case, the single cell echo developed in a relatively weak vertical wind shear and had a relatively simple kinematic structure. In this study, since we assumed the isolated echo had an axisymmetric or two-dimensional structure, its radial divergence field was utilized to infer the low-level divergence field. The vertical wind structure and in-cloud circulation were also calculated from RHI data assuming the clouds to have two-dimensional structures. Even if the calculated value is not quantitatively reliable, we believe that the circulation inferred using the RHI scan data can express a qualitatively reasonable wind field. For the second and third cases of rainbands, the vertical circulation was deduced in the same manner from the RHI frame perpendicular to the rainband. Numerical investigations by Tao and Soong (1986) and Tao and Simpson (1989) showed that two-dimensional circulation dominated the updraft in squall rainbands, whereas non-squall rainbands have three-dimensional circulation except in convective regions.

Since the organization and maintenance of convective regions of rainbands are influenced by convective outflows and cold pools generated by convective downdrafts (*e.g.*, Tao and Simpson, 1989), it is important to investigate the echo development process associated with the low-level wind field. Gust fronts (leading edges of convective outflow) were detected in rainbands using the criteria of Uyeda and Zrnic' (1986), who looked for a region of large Doppler velocity gradient. In this case study, we determined the gust front when the peak value of the Doppler velocity existed in front of the rain band. In addition to this, the vertical cross sections of the radar echoes were used to estimate the depth and origin of the convective outflow. In all cases, the 19 dBZ threshold echo area (elevation angle was 0° and 3°), the 19 dBZ echo top height, and the maximum reflectivity were estimated through their life cycle.

The environmental conditions were derived from sounding data obtained by omega sondes and an ISS (integrated sounding system) wind profiler. An overview of the cloud cluster development was derived from the GMS data. Vertical profiles of the potential temperature (θ), equivalent potential temperature (θ_e), saturated equivalent potential temperature (θ_e^*), CAPE, and vertical wind shear were calculated from the sounding data and ISS data. Omega sondes were launched four times a day at Momote (about 20 km east of the radar site; see Fig. 1 and Uyeda *et al.*, 1995) during the observation pe-

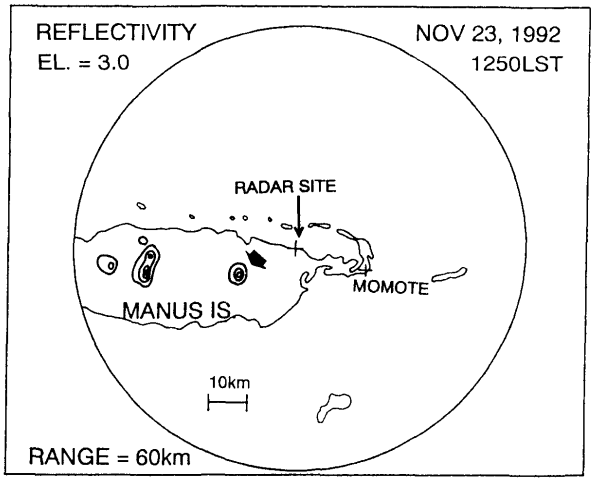

Fig. 1. Reflectivity of the PPI scan at 1250LST on November 23, 1992. Contours express the reflectivity from 19 dBZ in 4 dBZ intervals. The target echo of this study is indicated by the broad solid arrow. The coastline of Manus Island is expressed as a thin solid line. The location of the radar site was at the center of the figure, and the location of Momote (sounding and ISS station) is also depicted in this figure.

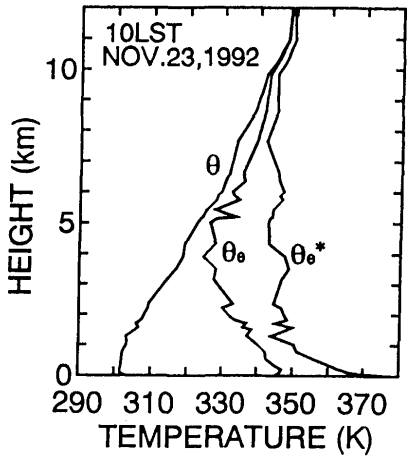

Fig. 2. Vertical profiles of potential temperature (θ), equivalent potential temperature (θ_e), and saturated equivalent potential temperature (θ_e^*) at Momote at 10LST on November 23, 1992.

riod. However, dew point data were not available in some sounding data on December 16 (second and third cases). The wind profiler data was obtained at 30-minute intervals.

3. Results

3.1 Life cycle of an isolated radar echo

During the Doppler radar observations on Manus Island, many isolated convective clouds (echoes) were observed over the island. These clouds were excited by strong solar radiation in the daytime. Figure 1 shows an example of a daytime isolated echo with a diameter of about 10 km in the PPI display of reflectivity. In this section, the isolated echo indicated by the solid arrow in Fig. 1 is examined in detail.

The atmospheric conditions (CAPE, vertical profile of θ_e, and vertical wind shear) of this case were calculated from the 10LST (LST = UTC + 10 hour) sounding at Momote. The CAPE was $\approx$ 1000 J/kg. Vertical profiles of θ, θ_e, and θ_e^* are shown in Fig. 2; a convectively unstable layer existed below 4 km and a dry layer existed below 7 km. The vertical wind shear between the surface and 4 km was 2.1×10^{-3} s^{-1}. These conditions correspond to a relatively low CAPE and low wind shear which were common atmospheric conditions in this study.

The echo transition is shown in Fig. 3 as a series of PPI scans (elevation angle = 3°) superimposed on the divergence (radial divergence) field. Since the echo was located 10–20 km from the radar site, as shown in Fig. 1, Fig. 3 expresses the echoes at altitudes between 0.5 km and 1 km. The echo moved very slowly ($\approx$ 2.5 m/s) from south to north, and we regarded it as almost stationary for the purpose of analysis. The divergence field showed the existence of a small convergent and divergent region in the early stages (1230 to 1250LST). The convergence field became dominant in the low-level wind field from 1250 to 1310LST, coinciding with the region of high reflectivity. At 1320LST, the divergent region appeared over the high reflectivity region, and subsequently increased in area to dominate the echo until the echo dissipated.

Figure 4 shows vertical cross-sections (reflectivity and Doppler velocity) of the echo along the lines indicated in Fig. 3. These cross-sections were selected as typical patterns during the echo's life cycle (except for the dissipating stage). In Fig. 4a (1236LST), the echo top was about 2 km high and the Doppler velocity was very small (the approaching and receding components were both less than 4 m/s). At 1313LST, the echo became taller at 1313LST with the echo top rising to about 6 km (Fig. 4b), and strong echo regions located at altitudes of 1 km and 2 km. The in-cloud wind (Doppler velocity) became faster, reaching a maximum Doppler velocity of over 10 m/s. The Doppler velocity field shows a clear 'lower level convergence-upper-level divergence' circulation. At 1321LST (Fig. 4c), the echo was still of high reflectivity at the lower level (between 2 km and 4 km in height), and an upper-level reflectivity core appeared at 6 km. The Doppler velocity field shows a similar circulation pattern to that of 1313LST (Fig. 4b), ex-

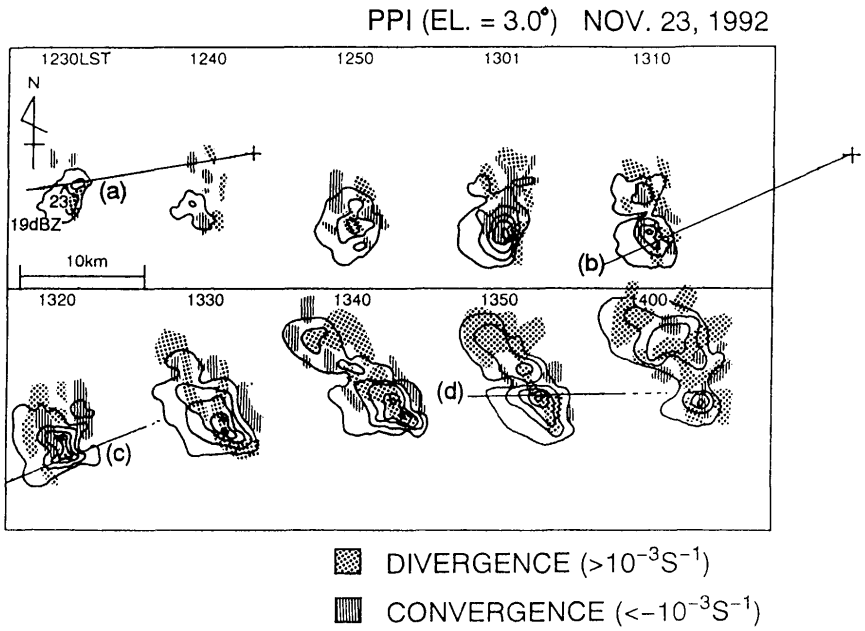

Fig. 3. Transition of the isolated echo indicated in Fig. 1 on November 23 at an elevation angle of 3°. Contours express the reflectivity from 19 dBZ in 4 dBZ intervals. Stippled areas express the radial divergence ($> 10^{-3}\cdot s^{-1}$), and hatched areas express the radial convergence ($< -10^{-3}\cdot s^{-1}$). The lines (a, b, c, and d) in this figure indicate the directions of the vertical cross section in Fig. 4.

cept for the appearance of upper-level divergent flow which coincided with the upper-level reflectivity core. In addition, a faster approaching wind component (convective outflow) greater than 6 m/s appeared near the surface. This wind component contributed to form the low-level divergence shown in Fig. 3. The echo top height was still increasing at 1348LST (Fig. 4d), by which time it had reached over 8 km in height, but the lower-level reflectivity became weaker and the echo broadened. The appearance of an anvil cloud was indicated by the Doppler velocity data which shows areas where the echo is less than 19 dBZ. The wind field had a simpler structure than the previous time (Fig. 4c), and the surface approaching component reduced its speed.

Figure 5 shows the transition of the echo area (threshold is 19 dBZ) counted from 3° elevation PPI data, including the transition of the 19 dBZ echo top height and maximum reflectivity. From Figs. 3, 4, and 5, we divided the life cycle of this isolated echo into five stages: 1) Appearance of the isolated echo: at this stage, the echo area (> 19 dBZ) was about 50 km^2 and the echo top height was less than 5 km. Analyses of the RHI scan data showed that in-cloud circulation (Doppler velocity field) was very weak. 2) The first clear circulation stage (around 1300LST): circulation below the melting level (about 4.5 km in height) became prominent, and produced a high-reflectivity echo. The low-level wind field was dominated by convergence. 3) The downdraft and appearance of an upper-level circulation stage (around 1320LST): the low level wind field became divergent as the downdraft started, while the circulation in the previous stage still existed. On the other hand, a new circulation (updraft) started at a height of 6 km and reached about 8 km in height. The maximum reflectivity appeared between Stages 2) and 3) below the melting level. 4) The maximum echo height stage: the echo top height reached its maximum (9.5 km in height), while the echo area was still increasing. Figure 5 shows that the echo top height did not increase continuously in this case. The reflectivity increased while the echo top height was stable around Stage 2). This result indicates that the low-level circulation contributed not to the vertical development of the echo but to the increase of the reflectivity at this stage. From the RHI scan data, the anvil cloud appeared to enlarge in the upper-level echo area. 5) The maximum echo area and dissipating stage: the echo area reached its maximum but the echo top height decreased rapidly, and then the echo dissipated rapidly. The RHI scan data (not shown) indicates that the echo became stratiform rather than convective. It is interesting to note that an anvil cloud appeared distinctly in such a small echo.

This analysis shows that isolated echoes, which had been thought to have simple structure and simple in-cloud circulation as shown by Rotunno *et al.* (1988), have somewhat complex structures and life cycles. It may be one of the characteristics of trop-

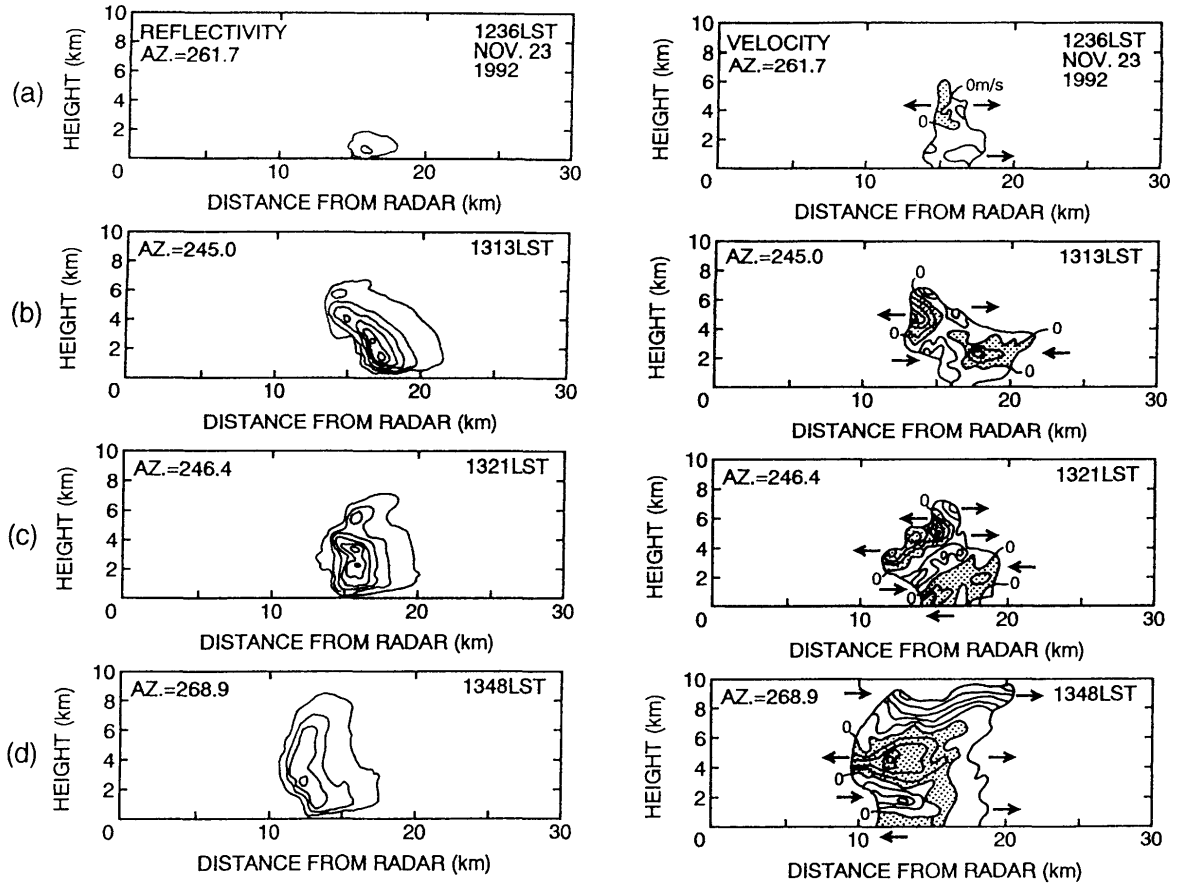

Fig. 4. Transition of vertical cross section (RHI) of reflectivity Doppler velocity of the echo along the lines indicated in Fig. 3, (a) 1236LST, (b) 1313LST, (c) 1321LST and (d) 1348LST. Contours indicate the reflectivity from 19 dBZ in 4 dBZ intervals and the Doppler velocity in 2 m/s intervals. The stippled area in the Doppler velocity indicates the velocity component approaching the radar.

ical isolated clouds. The details of the life cycle of this isolated echo are as follows. 1) There were two vertical circulations, one was below 4 km (note that the 0°C level was 4.5 km in height), and the other was around 6 km. Since the low-level high-reflectivity region continuously existed during the earlier stages, a warm-rain process was considered to be the major process for the production of rain at the earlier stages and an important mechanism of rain production in the tropics generally. 2) The occurrence of the downdraft coincided with the initiation of the upper level circulation. However, the physical relationship between the downdraft and the upper level circulation is still not clear. 3) The maximum echo area appeared at the dissipating stage. This is explained by the production and expansion of the anvil cloud in the upper level and the anvil cloud brought stratiform rainfall below it, thus the anvil cloud may have played a role in broadening the cloud area in the upper level (at 9 km altitude in this case).

3.2 Analysis of rainband (I) (13–18LST on December 16)

A rainband was observed from its initiation to its mature stage from 13 to 18LST on December 16, 1992. The atmospheric conditions in this case are shown in Fig. 6a, as θ, θ_e, and θ_e^* profiles at 10LST (3 hours before the echo initiation). The θ_e profile at this time was not available because of a fault in the sounding system. From the 22LST data (Fig. 6b), the CAPE was about 1300 J/kg; this value is not large by comparison with mid-latitudinal severe storms (2200~2500 J/kg, from Blustein and Jain, 1985). The time-height cross-section of wind from 12LST to 22LST derived from the ISS data is shown in Fig. 7. Since the echo was generated close to the island (see Fig. 8), the wind field at 12LST just represents the initial condition of the echo generation. At 12LST, the wind profile veers from the the surface to 4 km in height with relatively weak wind speed. At that time, the vertical wind shear from surface to 4 km in height was 2.8×10^{-3} s^{-1}. The low-level wind was accelerated from 14LST to 16LST with a maximum wind

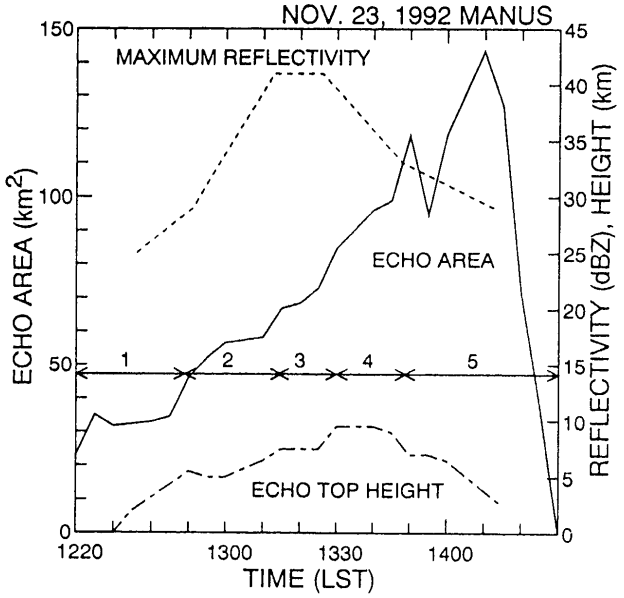

Fig. 5. Temporal variation of total echo area (> 19 dBZ), the 19 dBZ echo-top height, and the maximum reflectivity of the isolated echo shown in Figs. 3 and 4. Numbers (1–5) express the stages defined in the text.

speed of 17.5 m/s. Convective system circulation was considered to contribute to the acceleration of wind speed, because it coincided with a strong rear-to-front flow (Figs. 9a and 9b). The wind speed dropped after 16LST and this condition was the environmental condition of the next subsection.

Figure 8 shows the time series of PPI scans of reflectivity (elevation angle = 3°) from 1330LST to 1600LST. The first echo of the rainband was observed at 1300LST on the southern coast of Manus Island. At 1330LST in Fig. 8, several echo cells appeared. These echo cells and newly-generated echo cells formed an intense convective line (rainband) at 1400LST. The convective line was aligned east-to-west or east-southeast to west-southwest; the angle between this direction and the low-level shear vector (surface to 4 km) was almost parallel from the 10LST sounding data. The rainband propagated slowly to the south (≈ 4 m/s). From 14LST to 15LST, an intense echo area appeared toward the rear part of the rainband, because new echo cells appeared to the north of the old cells. This rainband extended in length and width with time. After 1500LST, the rainband reached a mature stage but had a relatively weak echo intensity. The strong echo area shifted to the central part or frontal part of the rainband. At this time, no new cell development occurred at the northern (rear) part of the rainband, and the rainband showed a stationary structure. At 1600LST, a stratiform region appeared to extend rearward (northward of the rainband from the higher elevation angle data).

Vertical cross sections along the lines in Fig. 8 are depicted in Fig. 9. These directions were almost perpendicular to the rainband. At 1358LST (Fig. 9a), a strong narrow echo existed in the rainband. Reflectivity cores were located at altitudes of 1 km, 4 km, and 8 km. The Doppler velocity data shows low-altitude (below 2 km) divergence, strong middle-altitude (2–5 km) convergence, and upper-level divergence. A strong approaching wind component contributed to low-level divergence which had a Doppler velocity greater than 12 m/s, while the environmental (ISS data in Fig. 7) low-level wind was less than 5 m/s. This difference between in-cloud wind and environmental wind caused new cells to develop to the north of the rainband, as mentioned in Fig. 8. This approaching wind was considered to be caused by convective downdraft.

At 1456LST (Fig. 9b, about one hour after Fig. 9a), the rainband had a similar structure to Fig. 9a, except for a relatively weak reflectivity, greater width, and reduced low-level divergent flow. A low level (~1 km) reflectivity core was not seen at this time. The weaker divergent wind made the generation of new cells inactive at the north edge of the rainband at this time (from 1500LST to 1530LST in Fig. 8). Doppler velocity data shows the echo top height was still increasing.

At 1559LST (Fig. 9c), the echo became broad, as shown in Fig. 8. Behind the strong echo area (convective region), a large stratiform echo area extended above the middle level (see the Doppler velocity data). The stratiform region extended with time to the northwest and covered almost all the radar range at the higher level after the convective region moved out of the radar range (not shown). The circulation structure was different from that of the earlier stages (Figs. 9a and 9b): a low-level rear-to-front wind (> 12 m/s) clearly appeared at this time and the updraft was mainly produced at the leading edge of the rainband (right edge of the rainband in Fig. 9c). The extension of the anvil area was clearly related to an upper-level easterly wind about 9 km in height. After that, this circulation of the echo was maintained. The echo-top height reached its maximum at this time, but the reflectivity was weaker than in the earlier stages.

In this case, the rainband was clearly related to a mesoscale cloud cluster. Figure 10 shows a time series of GMS IR images around Manus Island from 10LST to 22LST on December 16. At 10LST, a mesoscale cloud cluster had already formed southeast of Manus Island (indicated by the bold arrow in Fig. 10a). This cloud cluster was generated in a large-scale low-level confluence zone from the quick look stream line analysis data. This cloud cluster propagated northward and moved into the radar ob-

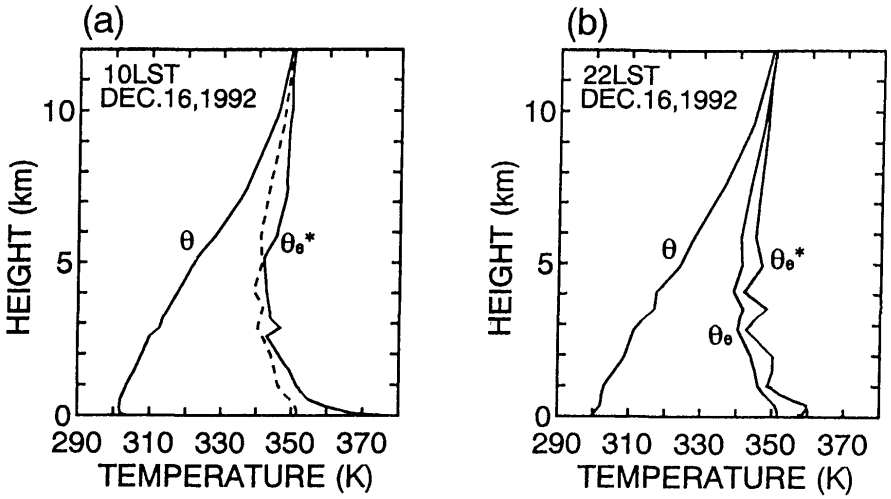

Fig. 6. Vertical profiles of potential temperature (θ), equivalent potential temperature (θ_e), and saturated equivalent potential temperature ($\theta_e{}^*$) of Momote at (a) 10LST and (b) 22LST on December 16, 1992. Because the θ_e profile at 10LST was not available, the e profile at 22LST is shown for reference by the dashed line in the 10LST profile.

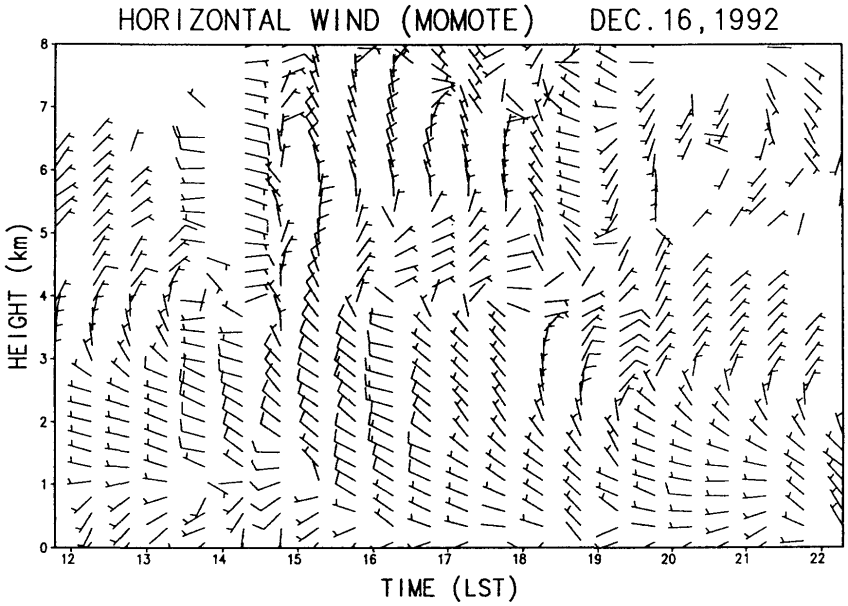

Fig. 7. Time-height cross section of wind from 12LST to 22LST on December 16, 1992, derived from the wind profiler (ISS) at Momote. In this figures full barbs indicate a speed of 10 m/s and half barbs indicate a speed of 5 m/s.

servation range (shown by the circle in the figure) at 14LST (Fig. 10b). The western narrow portion of the cloud cluster coincided with the early stage of the rainband. Therefore, this rainband was generated in the preexisting cloud cluster. At 18LST (Fig. 10c), a large area of low blackbody brightness temperature (T_{BB}) ($< -60°C$) extended over the radar observation range, coinciding with the stratiform region of the rainband. At this time, the region of low T_{BB} was recognized as a new cloud cluster with a horizontal scale of ~200 km. At 22LST (Fig. 10d), the cloud cluster moved northeast of Manus Island, while a newly-developed cloud cluster (indicated by the thin arrow in Fig. 10d) was located over the island. This new cloud cluster coincided with the rainband of the next subsection (3.3). It is interesting to note that the rainband propagated to the south, while the cloud cluster propagated to the north. This means that the low-level convergence region moved to the south, while the anvil region, which represents the low IR temperature area, was transported by the upper-level flow. This is related

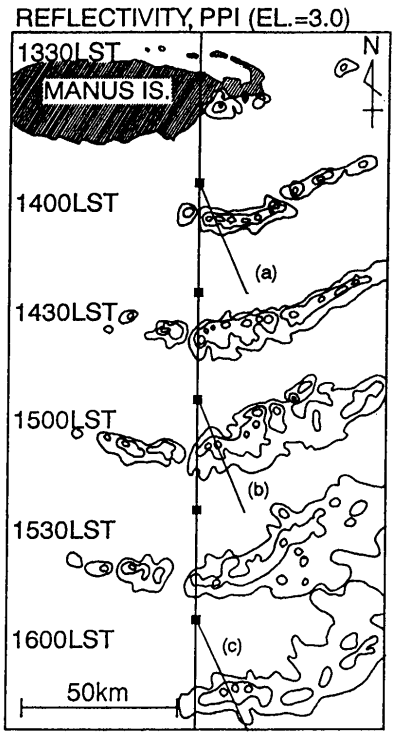

Fig. 8. Transition of a rainband in the PPI scan (elevation angle = 3°) in the case of Section 3.2 on December 16, 1992. Contours express the reflectivity from 19 dBZ in 8 dBZ intervals. The radar site in each scan is indicated by a black square. The shaded area indicates the location of Manus Island at 1330LST. Lines (a, b, and c) indicate the direction of the RHI scans in Fig. 9.

to the large scale circulation; the low-level wind was northerly or northwesterly and the upper-level wind was easterly. However, the anvil region might be maintained by a mesoscale updraft, as reported by Zipser *et al.* (1981), Gamache and Houze (1983), Houze and Rappaport (1984) and Tao and Simpson (1989). The relationship between the cloud cluster and rainband suggests that the rainband was initiated at the western portion of one cloud cluster and developed into a new cloud cluster.

3.3 Analysis of rainband (II) (20–23LST on December 16)

A narrower rainband appeared on December 16, 1992, just after the previous case. The vertical profiles of θ, θ_e, and $\theta_e{}^*$ at 22LST are shown in Fig. 6b. The e profile shows that a weak convectively unstable layer existed below 2.5 km, because (22LST) this time almost coincided with the passage of the rainband (see Fig. 11) over Momote (sounding station; see Fig. 1). Furthermore, weak rainfall was caused by the stratiform region of the rainband mentioned in Section 3.2. As mentioned in Section 3.2, the CAPE value at 22LST was about 1300 J/kg. The wind profile (Fig. 7) was different from the previous case; the southerly wind component which was seen in the previous case (from 12LST to 16LST) was absent, and instead a northwesterly wind dominated below 1 km. In this condition, the rainband appeared at the west-northwest boundary of the radar observation range.

Figure 11 shows the transition of the radar echo at an elevation angle of 0°, in 15-minute intervals. The rainband kept a relatively strong reflectivity till 2114LST, but the reflectivity of each cell varied dependent on time. The rainband was shorter than the previous case, and it consisted of several echo cells and a line oriented from southwest to northeast. This orientation almost coincided with the shear vector between the surface and 3.9 km in height. When the rainband appeared within the observation range (around 1958LST), the echo had already formed a narrow rainband. The rainband propagated east-southeast at a speed of 6 m/s, and each cell propagated in almost the same direction as the rainband (see cells a, b, and c in Fig. 11). After the rainband reached over the radar site (2129LST), the rainband became weaker. The rainband's (convective line's) orientation fluctuated with time; the orientation changed from southwest-northeast (SW-NE) at 1958LST, to west-east (W-E) at 2028LST, and finally to southwest-northeast (SW-NE) again at 2114LST. The transition of the line orientation was due to new cell formation, which was initiated by gust fronts.

Gust fronts were detected in the low-elevation PPI scans by the method mentioned in Section 2. The gust fronts are indicated by dashed lines in Fig. 11. At 1958LST, gust fronts were determined at the central part of the band and in front of the echo cell (c). However, no gust fronts were analyzed in front of the cell (a) and (b). At 2028LST, a new echo cell formed ahead of the gust front which was detected first at 1958LST. The formation of this cell changed the orientation of the rainband from SW-NE to W-E as noted above. At the same time, a new gust occurred in front of the cell (a). The rainband's orientation changed from W-E to SW-NE again at 2114LST. On this case, the times at which gust fronts occurred varied according to the development stage of each echo cell but it was confined to within 30 minutes (1958LST to 2028LST). Notice that the western part of the rainband at 2114LST, where the orientation did not change, was restrained in an eastward motion by the topography of Manus Island (see Fig. 11 at 2129LST where the coastline of Manus Island is depicted). Thus the orientation of the rainband was controlled by the gust front to some extent.

The development process and the initiation and signature of the gust front were examined by a se-

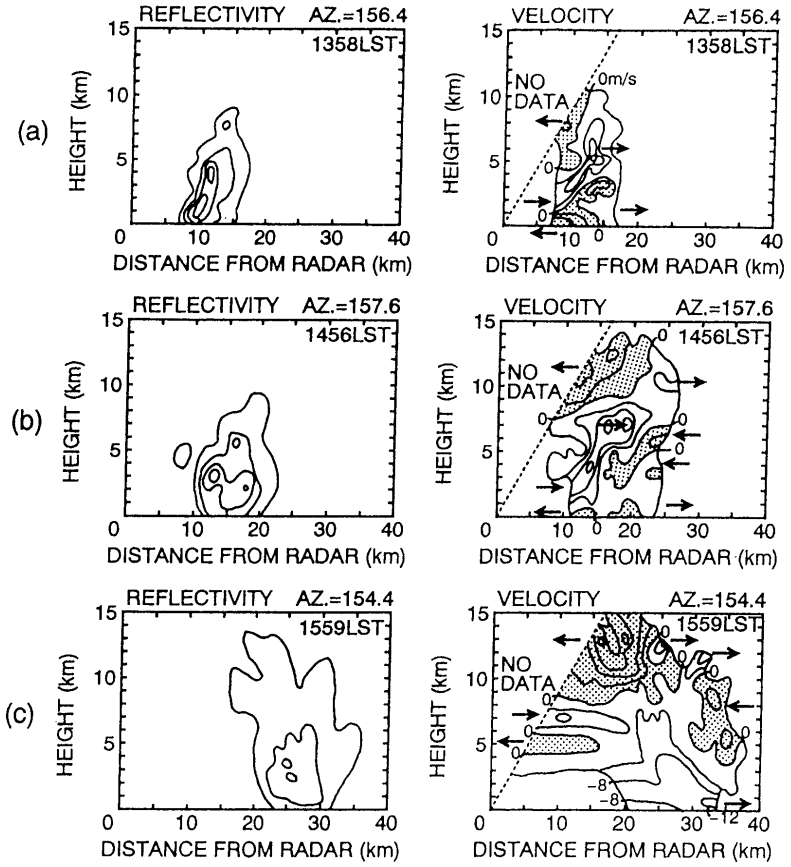

Fig. 9. Cross sections (RHI) of reflectivity and Doppler velocity along the lines indicated in Fig. 8 at (a) 1358LST, (b) 1456LST, and (c) 1559LST. Contours indicate the reflectivity from 19 dBZ in 8 dBZ intervals and 4 m/s intervals of Doppler velocity. The stippled area in the Doppler velocity indicates the velocity component approaching to the radar.

ries of vertical cross sections (RHI scans). Figure 12 shows the time series of the vertical cross section of the echo cell (a) (along the arrow in Fig. 11). As mentioned above, gust wind component was recognized as faster than 8 m/s; the fast-wind region (> 8 m/s) was stippled in the RHI frames in Fig. 12. At 1958LST, the echo reached its maximum reflectivity (> 34 dBZ) and the echo-top height (threshold is 19 dBZ) was 6.5 km. At this time, the fastest wind component (between 8 and 10 m/s) appeared at a height of 1.5 km, but did not reach the sea surface. At 2009LST, a strong-echo region descended to near the surface. On the other hand, the echo became broad with a faster wind component intruding into the central part of the echo.

As mentioned in the PPI data of Fig. 11, the gust front was detected at 2028LST in the echo cell (a). The vertical cross section at 2025LST shows that a fast wind component (> 8 m/s) reached the sea surface strong echo region, but the low-level reflectivity became weaker. This fast-wind component propagated slightly faster than the propagation speed of the gust-producing echo (6 m/s; see also 2039LST and 2053LST), causing cell generation in front of the gust-producing echo. By contrast, the echo top height increased rapidly (from 6.5 km to 8.5 km) at this time. This gust front existed at 2039LST and 2053LST with a speed of 12 m/s and a depth of 0.5 km to 1 km, and this faster wind region shifted to the frontal part of the echo. The faster wind component at 2 km altitude became weaker. The echo top height increased slowly and the anvil cloud began to form at 2053LST. After this time, the stratiform region extended over the radar coverage and the echo became weaker. A GMS IR image taken at 22LST (Fig. 10d) shows the eastern portion of a relatively small cloud cluster located over the radar observation range.

In-cloud circulation analysis calculated from Doppler velocity data (not shown) indicated that the updrafts mainly appeared in front of the gust front or at the boundary of the low-level rear-to-front flow (stippled area in Fig. 12). This circulation did not resemble the circulation in the mature stage of the rainband described in the previous subsection, because the low-level rear-to-front flow occurred intermittently rather than continuously as did the circulation in the previous case.

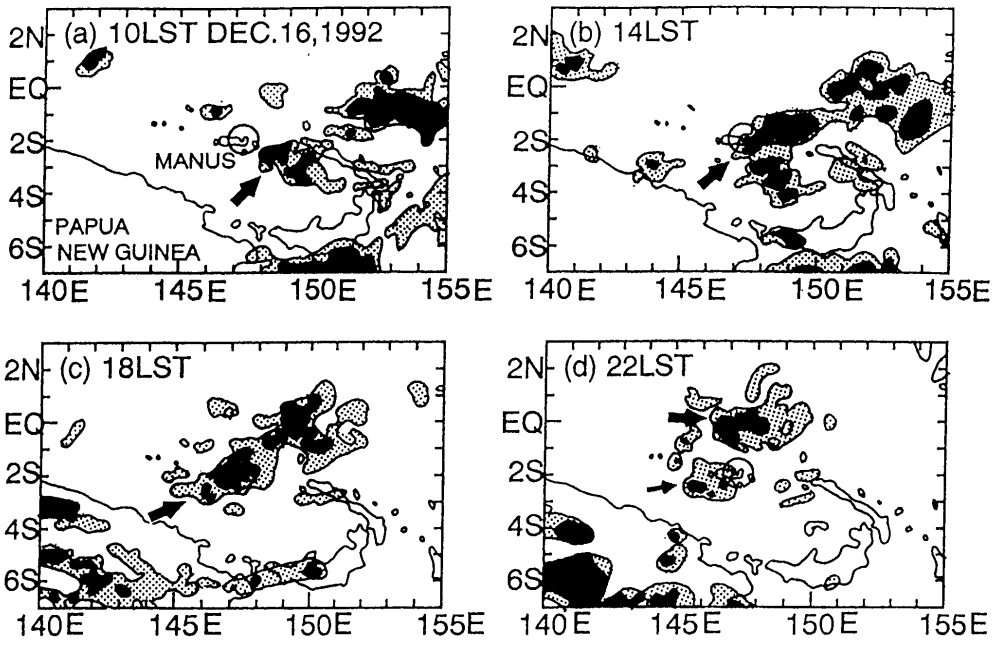

Fig. 10. GMS IR images around Manus Island at (a) 10LST, (b) 14LST, (c) 18LST, and (d) 22LST on December 16. The stippled area indicates a blackbody brightness temperature (T_{BB}) of less than $-40°C$, and the area where T_{BB} is less than $-60°C$ is shaded black. The circles in each frame indicate the radar observation range. The target cloud in Section 3.2 is indicated by bold arrows. The thin arrow in (d) indicates the target cloud in Section 3.3.

4. Discussion

4.1 Details of the rainbands

During GATE, convective systems were categorized into two types: squall (fast moving) systems and non-squall (slow moving) systems (Houze and Betts, 1981; Barnes and Sieckman, 1984). As mentioned in the introduction, squall systems have a fast propagation speed, an arc-shaped leading edge, and convective lines perpendicular to the low-level shear vectors. On the other hand, non-squall systems have a slow propagation speed and convective lines parallel to the low-level shear vectors. We applied these categories to the rainbands of this case study.

The rainband in Section 3.2 was slow-moving (non-squall) because it had a convective line almost parallel to the low-level shear vector. Figure 13 shows a wind hodograph relative to the surface wind at 10LST, 12LST, 14LST, and 16LST on December 16. At 10LST (before the initiation of the rainband), the shear vector which represents the environmental condition of this case was almost parallel to the line orientation. At 12LST, 14LST, and 16LST, the shear vector became perpendicular to the line under the influence of the convective activity. The interaction between the environment and the convective system was not clarified in this study.

The rainband of Section 3.3 was also a non-squall system, because the rainband was almost parallel to the shear vector, but it had a rather faster propagation speed than the previous case. Figure 14 shows shear vectors from 1917LST to 2317LST on December 16. In this case, the ISS station was located 45 km ahead of the rainband at 20LST. The shear vector was clearly parallel to the line orientation when the ISS station was far away from the rainband (1917LST and 2017LST) and just ahead of the rainband (2117LST). However, just after the passage of the rainband (behind the rainband. at 2217LST and 2317LST), the shear vector was perpendicular to the rainband as in the previous case. Zipser *et al.* (1981) showed that non-squall-type rainbands propagated perpendicularly to the shear vector, while individual cells propagated parallel to the rainband. In this case, however, the rainband and individual convective cells both propagated perpendicular to the rainband.

Although both rainbands were categorized as non-squall systems, they had different circulation structures and propagation speeds. As mentioned in Sections 3.2 and 3.3, a stationary circulation structure appeared in the case of Section 3.2, but the circulation was not so clear in the case of Section 3.3. The rainband of Section 3.3 had a faster propagation speed than the rainband of Section 3.2.

4.2 Comparison of life cycles

In order to find the common element of these three case studies, we compared the temporal variation of their echo areas (19 dBZ threshold), 19 dBZ echo top

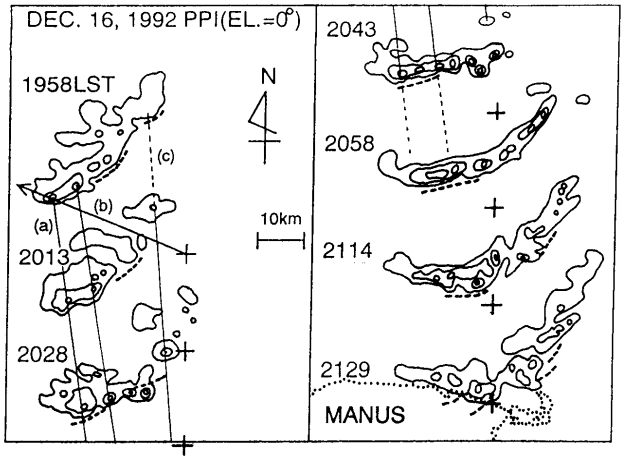

Fig. 11. Transition of a rainband in the PPI scan (elevation angle = 0°) from 1958LST to 2129LST on December 16, 1992. Contours express the reflectivity from 19 dBZ in 8 dBZ intervals. Dashed lines indicate the gust fronts. The plus symbols indicate the location of the radar at each time. The arrow from the symbol at 1958LST indicates the direction of the RHI scan in Fig. 12. The lines express the corresponding echo cells a, b, and c. The coastline of Manus Island is indicated by the dotted line in the 2129LST echo.

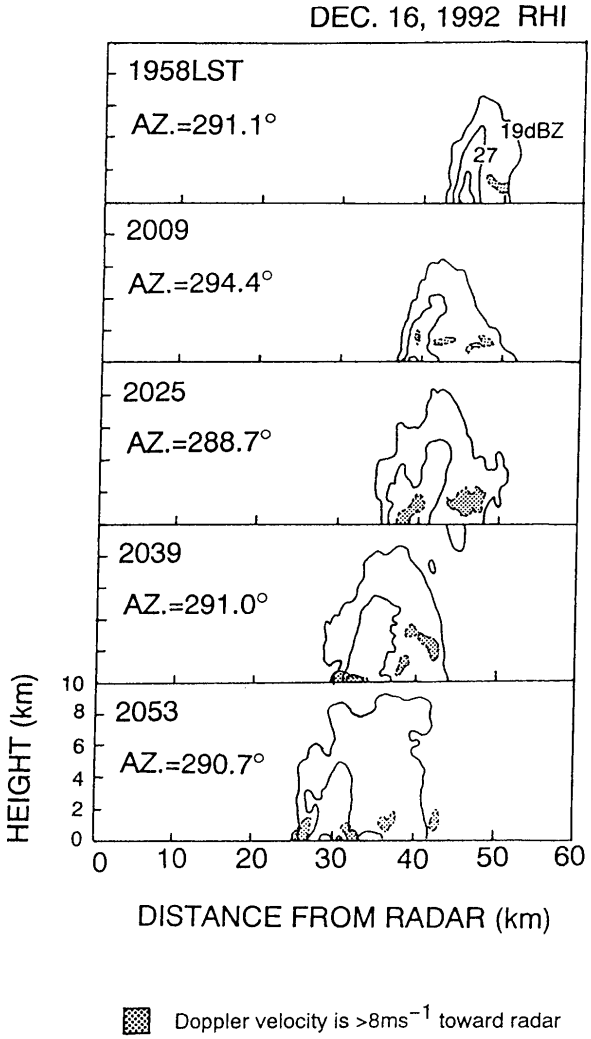

Fig. 12. Transition of vertical cross section (RHI) of cell (a) in Fig. 11. Contours indicate the reflectivity from 19 dBZ in 8 dBZ intervals. Stippled areas indicate a Doppler velocity faster than 8 m/s toward the radar.

heights, and maximum reflectivities. The temporal variation of the echo area, the echo top height and maximum reflectivity of the second and the third cases (Sections 3.2 and 3.3) are summarized in Fig. 15 in the same manner as in Fig. 5. On December 16, 1992, a larger-scale rainband (Section 3.2) appeared during the daytime, followed by the rainband of Section 3.3, which appeared at night. Like the case of the isolated echo (Fig. 5), the peak of maximum reflectivity appeared first. In both cases, the maximum reflectivity appeared in the lower part of the echoes (below the melting level). The time taken to reach maximum reflectivity is almost the same in all three cases (about 45 minutes from the first echo; but the initial time of the case in Section 3.3 is not ambiguous). As inferred in Section 3.1, the peak of maximum reflectivity was considered to be related to a warm rain process and it dominated the earlier stage of the cloud development. As mentioned in Section 3, the CAPE values of all these cases are relatively low (less than 1300 J/kg), resulting in slow development at early stages. This result influences the transition of echo-top height.

The peaks of the echo-top heights appeared after the echoes reached maximum reflectivity (at low level). These peaks coincided with the generation of upper-level circulation, as described in Section 3.1, the formation of a stationary convective line (the appearance of low-level rear-to-front flow) in Section 3.2, and the rapid development of echo at the same time as convective outflow occurred in Section 3.3. In Section 3.1, the echo-top height reached the first peak of 5.5 km in height (30 minutes from the fast echo in Fig. 5), after which the echo-top height slightly decreased for 15 minutes and increased again to reach a stable altitude of about 7.5 km. Finally, the echo-top height increased again and reached the maximum height. In Section 3.2 (Fig. 15), a stable echo top height did not appear before the maximum, but a low rate of increase of echo-top height appeared when the echo-top height was between 7 km and 10 km. In Section 3.3, since the echo did not initially appear within the observation area, we did not know the earlier development process. However,

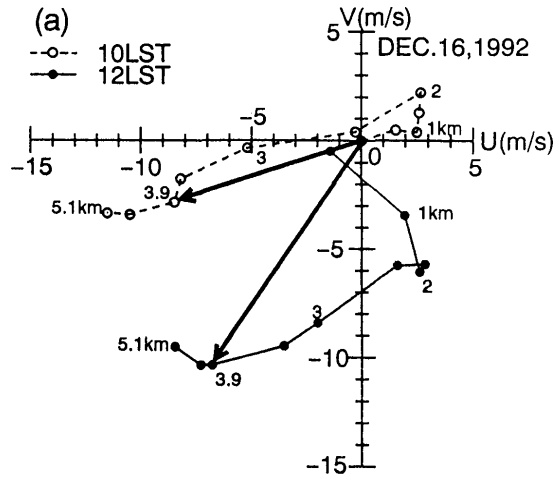

Fig. 13. Wind hodograph relative to surface wind (a) at 10LST and 12LST and (b) at 14LST and 16LST at Momote derived from the ISS wind profiler. Arrows indicate the shear vector from the surface to 3.9 km in height.

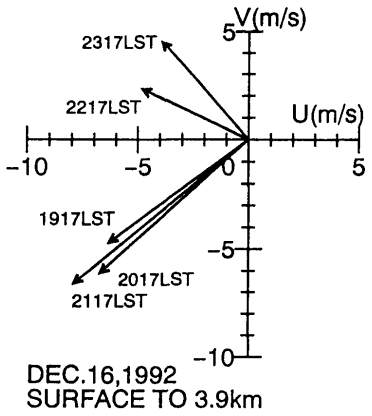

Fig. 14. Shear vectors from the surface to 3.9 km in height from 1917LST to 2317LST on December 16, 1992, derived from the ISS wind profiler.

the tendency of echo-top height increase was similar to the case of Section 3.1; after a stable situation of 5~6 km in height, the echo top height increased. The maximum reflectivity (at the low level) appeared after the echo height became stable. It is explained that precipitation particles which were continuously produced by the low-level updraft were restrained from vertical development at this time, and worked to intensify the low level reflectivity.

After reaching the maximum echo-top height, the echo area increased rapidly. This was mainly caused by the appearance of the anvil cloud. Thus, the maximum echo area appeared after the peak of the maximum echo-top height. In other words, the echo area was mainly occupied by a stratiform anvil cloud at the later stages of the rainbands. It is worth emphasizing that a small echo such as Section 3.1, also developed into an anvil cloud. This may be one of the characteristics of tropical clouds. As shown in Section 3.2, the appearance of a low T_{BB} area coincided with the development of a stratiform (anvil) region. Note that the echo area at the early stage of the rainband of Section 3.3 (375 to 465 minutes in Fig. 15) represents the rainbands of both Sections 3.2 and 3.3. By this reason, the echo area of the rainband of Section 3.3 was considered to increase monotonically at its early stage, like other cases. The time lags from the maximum echo-top height to the maximum echo area were also proportional to the horizontal scale.

4.3 Convective outflows (gust fronts)

Convective outflows were observed in each case, but at different stages in their life cycles. In the case of an isolated echo, convective outflow occurred just after the time of maximum (low-level) reflectivity. In addition, the occurrence of the convective outflow coincided with the start of upper-level circulation (the time of rapid development). In the rainband of Section 3.2, convective outflow occurred at the earlier stage and at the mature stage as front-to-rear and rear-to-front directions, respectively.

On the other hand, convective outflow occurred significantly after the maximum reflectivity appeared in the rainband of Section 3.3. In this case, the gust coincided with rapid development of the echo to a higher level between 2009LST (echo top height = 6 km) and 2025LST (echo top = 8.5 km). The strong surface wind (maximum wind speed was 12 m/s) was inferred to be transported from about 2 km in height (wind speed was 8~10 m/s). Therefore, the surface wind was slightly accelerated. It is caused by the relatively moist tropical oceanic atmosphere, *i.e.*, the acceleration effect of evaporative

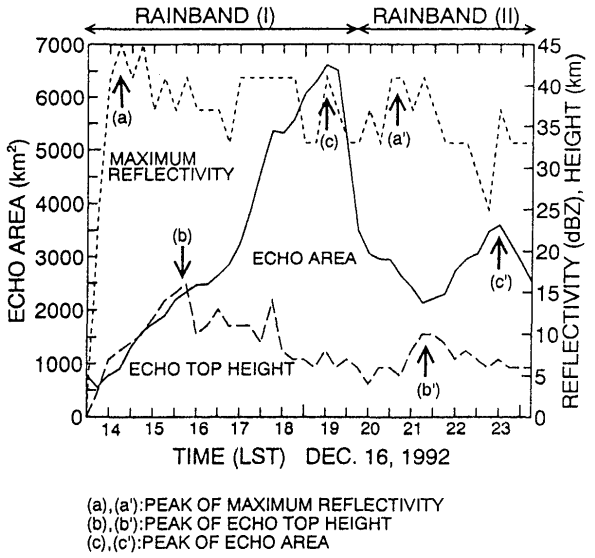

Fig. 15. Temporal variation of total echo area (> 19 dBZ), 19 dBZ echo top height, and maximum reflectivity of rainbands on December 16, 1992.

cooling is not large. The wind gust in front of the echo cell (a) occurred only once, although the gust component remained near the surface for more than 30 minutes.

The relative position of the gust front from the rainband was just in front of the rainband, even if the gust had a faster wind component. This feature is similar to the result obtained by Tao and Simpson (1989) in their numerical investigation of tropical non-squall rainbands.

5. Concluding remarks

In this paper, we have revealed some characteristics of tropical convective clouds from three case studies. The common features of the case studies were examined in term of the time taken for the maximum reflectivity of the echo to appear, the maximum echo top height, and the maximum echo area. Echoes were developed under conditions of low CAPE (< 1300 J/kg) and low vertical wind shear (2.8×10^{-3} s^{-1}).

The life cycle of an isolated echo showed a clear division between low-level circulation and upper-level circulation. In the earlier stage, low-level circulation dominated in the echo. Maximum reflectivity appeared at this stage, suggesting that a warm-rain process was dominant. After the echo reached maximum reflectivity, a downdraft occurred and upper-level circulation began; it is not clear whether or not these phenomena are linked. The maximum echo top appeared at this stage and the anvil cloud then began to grow. After the appearance of the anvil cloud, the echo area rapidly increased, but convective activity weakened, and the echo changed to stratiform.

These characteristics also appeared in other cases. For rainbands, the maximum reflectivity appeared about 45 60 minutes after the first echo. Next, the maximum echo-top height appeared, but the time lag from the maximum reflectivity varied from one case to the next, perhaps due to differences in the maximum echo-top heights. The maximum echo area appeared significantly after the maximum echo-top height, and was mainly occupied by stratiform regions.

Rainbands were distinguished as squall systems or non-squall systems. Both rainbands were categorized as non-squall systems because the convective line was parallel to the low level shear vector. The propagation speed of the first case (Section 3.2) was rather slow (4 m/s). The propagation speed of the second rainband (Section 3.3) was faster than the first one (6 m/s).

Convective outflows were observed in all cases. In particular, a gust front was observed in the rainband of Section 3.3. The gust front was characterized by a thickness of 0.5 to 1.0 km and a propagation speed of 8 to 10 m/s. The gust front was constantly positioned in front of the rainband. In this case, the gust front propagated slightly faster than the rainband. The rainband in Section 3.2 showed two distinct convective outflows: one occurred during the developing stage, and the other occurred during the mature stage as a continuous rear-to-front flow (Houze, 1977) and it contributed to maintaining the rainband.

Acknowledgments

The authors express their thanks to the members of J-COARE radar observation group in Manus Island for their hard work during the radar observation, and also to the National Weather Service, Papua New Guinea for its cooperation. We are grateful to the Japan Marine Science and Technology Center for their assistance in transportation of equipment to Manus Island, Papua New Guinea. We would like to thank Professor Katsuhiro Kikuchi for his encouragement through out this study. The authors also appreciate critical comments by three anonymous reviewers. This study was supported by the Grant-in-Aid for Scientific Research from the Ministry of Education, Science and Culture of Japan (No. 06NP021).

References

Barnes, G.M. and K. Sieckman, 1984: The environment of fast- and slow-moving tropical mesoscale convective cloud lines. *Mon. Wea. Rev.*, **112**, 1782–1794.

Bluestein, H.B. and M.H. Jain, 1985: Formation of mesoscale lines of precipitation : Severe squall lines

in Oklahoma during the spring. *J. Atmos. Sci.*, **42**, 1711–1732.

Chong, M., P. Amayenc, G. Scialom and J. Testude, 1987: A tropical squall line observed during COPT 81 experiment in West Africa. Part I: Kinematic structure inferred from dual-Doppler radar data. *Mon. Wea. Rev.*, **115**, 670–694.

Gamache, J.F. and R.A. Houze, Jr., 1983: Water budget of a mesoscale convective system in the tropics. *J. Atmos. Sci.*, **40**, 1835–1850.

Hobbs, P.V. and O.G. Persson, 1982: The mesoscale and microscale structure and organization of clouds and precipitation in midlatitude cyclones. Part V: The substructure of narrow cold frontal rainbands. *J. Atmos. Sci.*, **39**, 280–295.

Houze, R.A., Jr., 1977: Structure and dynamics of a tropical squall-line system. *Mon. Wea. Rev.*, **105**, 1540–1567.

Houze, R.A., Jr. and A.K. Betts, 1981: Convection in GATE. *Rev. Geophys. Space Phys.*, **16**, 591–576.

Houze, R.A., Jr., S.G. Geotis, F.D. Marks, Jr. and A.K. West, 1981: Winter monsoon convection in the vicinity of north Borneo, Part I: Structure and time variation of the clouds and precipitation. *Mon. Wea. Rev.*, **109**, 1595–1614.

Houze, R.A., Jr. and E.N. Rappaport, 1984: Air motion and precipitation structure of an early summer squall line over the eastern tropical Atlantic. *J. Atmos. Sci.*, **41**, 553–574.

Keenan, T.D. and S.A. Rutledge, 1993: Mesoscale characteristic of monsoonal convection and associated stratiform precipitation. *Mon. Wea. Rev.*, **121**, 352–374.

Leary, C.A. and R.A. Houze, Jr., 1979a: The structure and evolution of convection in a tropical cloud cluster. *J. Atmos. Sci.*, **36**, 437–457.

Leary, C.A. and R.A. Houze, Jr., 1979b: Melting and evaporation of hydrometeors in precipitation from the anvil clouds of deep tropical convection. *J. Atmos. Sci.*, **36**, 669–697.

Mori, K., 1992: Internal structure and time evolution of a cloud cluster in the western tropical pacific region observed by Keifu Maru. *J. Meteor. Soc. Japan*, **70**, 1111–1123.

Rotunno, R., J.B. Klemp and M.L. Weisman, 1988: A theory for strong, long-lived squall lines. *J. Atmos. Sci.*, **45**, 463–485.

Tabata, A., S. Nakazawa, Y. Yasutomi, H. Sakakibara, M. Ishihara and K. Akaeda, 1989: The structure of a long-lasting single cell convective cloud. *Tenki*, **36**, 499–507 (in Japanese).

Tao, W.-K. and S.-T. Soong, 1986: A study of the response of deep tropical mesoscale processes: Three dimensional numerical experiments. *J. Atmos. Sci.*, **43**, 2653–2676.

Tao, W.-K. and J. Simpson, 1989: Modeling study of a tropical squall-type convective line. *J. Atmos. Sci.*, **46**, 177–202.

Uyeda, H. and D. Zrnic', 1986: Automatic detection of gust fronts. *J. Atmos. Oceanic Technol.*, **3**, 36–50.

Uyeda, H., Y. Asuma, N. Takahashi, S. Shimizu, O. Kikuchi, A. Kinoshita, S. Matsuoka, M. Katsumata, K. Takeuchi, T. Endoh, M. Ohi, S. Satoh, Y. Tachibana, T. Ushiyama, Y. Fujiyoshi, R. Shirooka, N. Nishi, T. Tomita, H. Ueda, T. Sueda, and A. Sumi 1995: Doppler radar observations on the structure and characteristics of tropical clouds during the TOGA-COARE IOP in Manus, Papua New Guinea — Outline of the observation —. *J. Meteor. Soc. Japan*, **73**, 415–426.

Zipser, E.J., 1977: Mesoscale and convective-scale downdrafts as distinct components of squall line structure. *Mon. Wea. Rev.*, **105**, 1568–1589.

Zipser, E.J., R.J. Mertin and M.A. LeMone, 1981: Mesoscale motion fields associated with a slowly moving GATE convective band. *J. Atmos. Sci.*, **38**, 1725–1750.

TOGA-COARE 集中観測期間中のパプアニューギニア、マヌス島における雲群の構造に関するドップラーレーダー観測：1992 年 11 月 23 日と 12 月 16 日に観測された 3 つのケーススタディ

高橋暢宏[1]・上田　博

(北海道大学理学部)

TOGA-COARE の集中観測期間中には様々なタイプの雲がマヌス島に設置したドップラーレーダーによって観測された。本論文では孤立対流雲と 2 種類のレインバンドを解析し、それらの特徴をエコー面積、エコー頂高度、最大反射強度の時間変化の観点から明らかにした。ケーススタディから得られた共通する特徴は、1) 最大反射強度のピークはライフサイクル中の早いステージで現れ、それは下層の循環によってもたらされた。2) エコー頂のピークは最大反射強度のピークにやや遅れて現れ、これは上層の循環のステージの急激な発達に対応していた。3) アンビルの出現によるエコー面積のピークが最後に現れた。

[1]現在所属：通信総合研究所

孤立エコーのケースでは、上記の特徴が運動学的に細かく解析された。このケースでは下層の循環のステージから上層の循環のステージへの移行が現れた。これらは、ドップラー速度場の解析から運動学的にも矛盾なく説明された。また、上層の循環のステージで最大エコー頂までに発達した後にアンビル雲が発達しエコー面積が最大になり、層状降水をもたらした。

2つのレインバンドのケースは、ノンスコールタイプに分類された。一方は遅く伝播し、継続的な下層の後面から前面に向かう流れが成熟期に現れた。もう一方は、やや速い伝播速度を持っていたが、後面から前面へ向かう流れは継続的でなかった。それぞれは、GATE 期間中に観測されたものの特徴と必ずしも一致していなかった。また、convective outflow は、いずれのケースにも観測され、2つめのレインバンドのケースではガストフロントとして観測されたものもあった。 このガストフロントは 0.5 km~1 km の厚さを持ち伝播速度は 8~10 m/s であり、これは、レインバンドの伝播速度よりやや速く、ガストフロントはレインバンドのすぐ前方に位置していた。